Nematic to smectic texture transformation in MBBA by *in situ* synthesis of silver nanoparticles†

P. K. Sudhadevi Antharjanam* and Edamana Prasad*

Received (in Gainesville, FL, USA) 13th May 2009, Accepted 2nd December 2009
First published as an Advance Article on the web 29th January 2010
DOI: 10.1039/b909428h

The present study describes the texture changes in 'nematic' *N*-(4-methoxybenzylidene)-4-butylaniline (MBBA) by *in situ* synthesis of silver nanoparticles in the system without any external reducing or stabilizing agents. Optical polarizing microscopy (OPM), differential scanning calorimetry (DSC), nuclear magnetic resonance (NMR) spectroscopy, Fourier-transform infrared (FT-IR) spectroscopy, and scanning and transmission electron microscopy (SEM and TEM) were utilized to understand the mechanistic details of the texture transformation in MBBA. The experimental results collectively suggest that the silver nanoparticles are generated through the reduction of silver ions by MBBA upon heat treatment, followed by a clear texture transformation from 'nematic' to 'smectic'. The 'smectic' MBBA–Ag NP conjugate forms a stable luminescent glassy phase on rapid cooling, with an emission maximum of 500 nm upon photo-excitation at the silver plasmon absorption.

Introduction

The formation of nanoparticles in a liquid crystal (LC) medium has been recognized as a promising arsenal for materials chemists to tune the properties of matter at the nano dimension.[1–8] Since liquid crystals possess order at the molecular (*nano*) level, and the properties of nanoparticles are extremely dependant on the perseverance of their uniform size/shape, generating and incorporating nanoparticles into LC phases provides great opportunities to design functional materials that have direct applications in display systems, ferroelectric materials, and photonics.[9,10] Recent reports of the preparation of polymeric nanostructures of fluorinated acrylates in a condensed smectic phase and leaf-like gold nanostructures from imidazolium lamellar LCs containing dicyanoaurate counter ions suggest that nanoparticle formation in LC phases is a highly feasible process.[11,12] The elegant works of Lattermann and co-workers have shown that copper nanoparticles with 3 nm diameter can be synthesized by reducing copper(II) complexes in hexagonal columnar poly(propyleneimine) dendrimer-based LCs.[13] *In situ* formation of gold nanoparticles embedded in glassy liquid crystals of amine-containing cholesterols has also been reported.[10] The impact of nanoscale particles and carbon nanotubes in liquid crystal display systems has been recently highlighted by Qi and Hegmann.[14]

While the use of lyotropic LC materials in the preparation of silver nanoparticles has been extensively studied, the formation and stabilization of silver nanoparticles in thermotropic mesophases have been rarely reported.[15] Barmatov and co-workers describe the *in situ* synthesis of silver nanoparticles in a polymer matrix and its effect on the clearing temperature, as well as the mesophase temperature interval.[16a] It has been recently reported that some of the mesogenic silver nanocomposites exhibit interesting conductivity properties.[16b] Liquid crystalline capped silver–palladium bimetallic nanoparticles were prepared and their electro-optical properties were studied by Toshima and co-workers.[16c] While *in situ* synthesis of silver nanoparticles in the LC state results in many useful material properties, to the best of our knowledge, texture transformation in mesogenic systems induced by silver nanoparticles has not been reported.

Herein, we describe, for the first time, the observation of *in situ* nanoparticle-induced 'nematic' to 'smectic' texture transformation in a room temperature liquid crystal, *N*-(4-methoxybenzylidene)-4-butylaniline (MBBA). The silver nanoparticles were generated through the reduction of silver ions by MBBA upon heat treatment, which induced a texture change for the mesogenic material. Interestingly, the smectic phase of the MBBA–Ag NP conjugate can be preserved in a glassy state upon rapid cooling of the system from higher temperatures. Most excitingly, photoluminescence was observed from MBBA–Ag NP conjugate in the green region of the visible spectrum upon excitation at 420 nm in the glassy phase. The intensity of the emission was found to be proportional to the amount of nanoparticle precursor used, suggesting that the emission originated from the silver nanoparticles generated in the LC phase.

Results and discussions

Amines such as 4-aminophenol, 2-methyl aniline and oleyl amine are known to reduce silver and gold ions in solution to the corresponding nanoparticles.[17] Amine-containing dendrimers,

Department of Chemistry, Indian Institute of Technology Madras (IITM), Chennai, India 600 036.
E-mail: santharjanam@rediffmail.com, pre@iitm.ac.in;
Fax: +91 44-2257-4202; Tel: +91 44-2257-4232

† Electronic supplementary information (ESI) available: UV-Vis spectra, SEM and TEM images, OPM pictures, and fluorescence spectra of MBBA–Ag NP conjugate at different mol% $AgNO_3$, FT-IR spectra of MBBA–Ag NP conjugate, fluorescence spectra for the control experiments described in the text. See DOI: 10.1039/b909428h.

such as poly(amidoamine) {PAMAM}, are also capable of generating silver nanoparticles by the reduction of silver ions through single electron transfer reduction from the large number of amines present in the dendritic systems.[18] Since the reduction of silver ions by amines to nano-silver is exothermic, heat treatment or UV irradiation of the reaction mixture is generally required. Since MBBA contains an imine nitrogen capable of donating electrons, we explored its ability to reduce silver ions, forming silver nanoparticles *in situ*, hoping that the LC arrangement will stabilize the generated nanoparticles. For that, a homogeneous solution of MBBA (0.15 mmol) and silver nitrate (1, 3, 5 and 80 mol%) in 5 mL methanol was drop-cast onto a glass slide and the solvent was allowed to evaporate. After drying, the plate was heated to isotropic temperature and kept at this point for 2 min. On heating, the initially colorless film turned to light brown, indicating the reduction of silver nitrate. Fig. 1 contains the thin film absorption spectra of MBBA and the MBBA–$AgNO_3$ mixture prepared using 5 mol% silver nitrate after heat treatment. The UV-Vis absorption spectrum shows a broad peak between 400–470 nm, corresponding to the silver plasmon absorption.

The silver plasmon absorption peak undergoes a slight bathochromic shift upon increasing the concentration of $AgNO_3$. The absorption spectra with different molar ratios of MBBA and $AgNO_3$ exhibited similar features, and the spectra retained their shape for several days, indicating that silver nanoparticles are not aggregating in the mesophase. The formation of silver nanoparticles (Ag NPs) in MBBA host systems was further confirmed by scanning electron microscopy (SEM) and transmission electron microscopy (TEM). The SEM image of the MBBA–Ag NP conjugate prepared using 80 mol% $AgNO_3$ is shown in Fig. 2a. The TEM image of the corresponding system shows the presence of silver nanoparticles and nanorods with lower aspect ratio (Fig. 2b).

The size of the Ag nanoparticles in the TEM image was in the range of 20–95 nm. SEM and TEM images for MBBA–Ag NP conjugates prepared using various molar ratios of $AgNO_3$ are given in the ESI (Fig. S3–S5).†

Fig. 3 shows the X-ray diffraction (XRD) pattern of the MBBA–Ag NP conjugate (MBBA + 80 mol% $AgNO_3$) deposited on a glass substrate. It shows the diffraction peaks at 2θ = 38.1, 44.3, 64.5 and 77.4°, corresponding to the reflections of [111], [200], [220] and [113] planes for the cubic Ag phase. The lattice constant for the cubic cell was 4.08 Å, which is in good agreement with the reported data for pure silver.[19] Crystallite sizes were calculated from the silver (111) diffraction line using Scherrer's equation: $L = K\lambda/\beta \cos\theta$, where L is the mean dimension of the crystallite, β is the full width at half maximum intensity of the diffraction peak, θ is the diffraction angle, λ is the wavelength of the Cu-Kα radiation (0.1540 nm) and the K value is taken as 0.89. The value obtained was 23 nm, which is lower than that of the average size obtained from TEM images (50 nm). The increased size obtained in TEM images could be due to the presence of the capping organic moieties coordinated to the nanoparticles (*vide infra*).

To understand the effect of the silver nanoparticles on the LC behavior of MBBA, we studied the phase transitions of MBBA–Ag NP conjugate films using an optical polarizing microscope (OPM) and differential scanning calorimetry (DSC). The mixtures containing 1, 3 and 5 mol% $AgNO_3$ showed identical texture properties under OPM. While the mesogen MBBA shows room temperature nematic texture, with a clearing temperature of 35 °C, the texture was lost in the presence of 1, 3 and 5 mol% $AgNO_3$. Fig. 4 shows characteristic optical polarizing microscopic pictures of an MBBA–Ag NP conjugate prepared using 5 mol% $AgNO_3$.

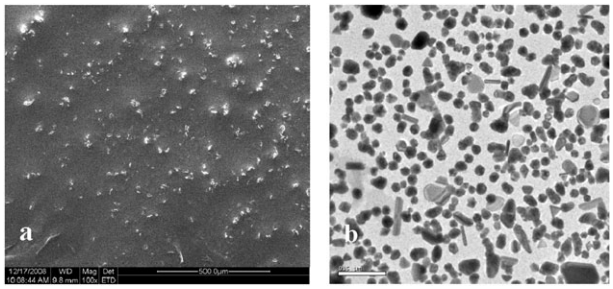

Fig. 2 SEM and TEM images of the MBBA–Ag NP conjugate (a and b, respectively) prepared using 80 mol% $AgNO_3$. Scale bar for SEM and TEM are 500 μm and 500 nm, respectively.

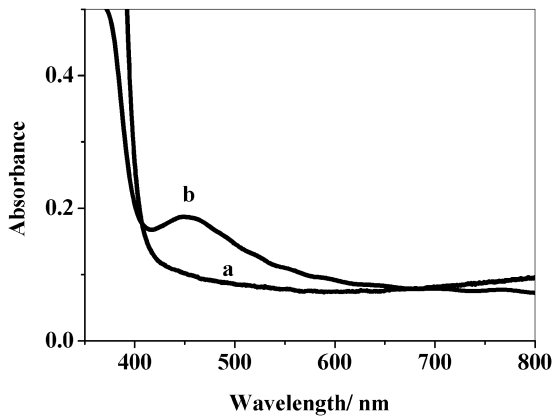

Fig. 1 UV-Visible thin film absorption spectra of (a) MBBA alone, and (b) the MBBA–$AgNO_3$ mixture prepared using 5 mol% $AgNO_3$, after heating to isotropic temperature and cooling.

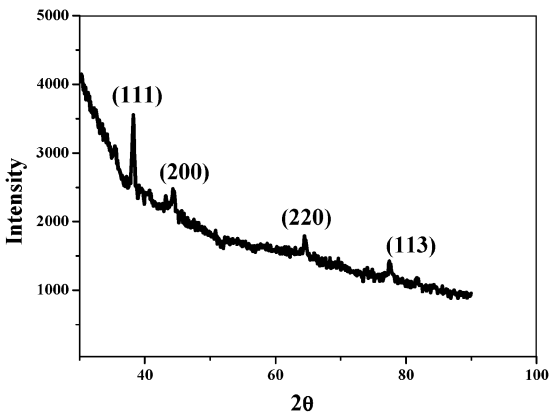

Fig. 3 XRD pattern for silver nanoparticles generated in the MBBA liquid crystalline domain. 80 mol% $AgNO_3$ was used in this case.

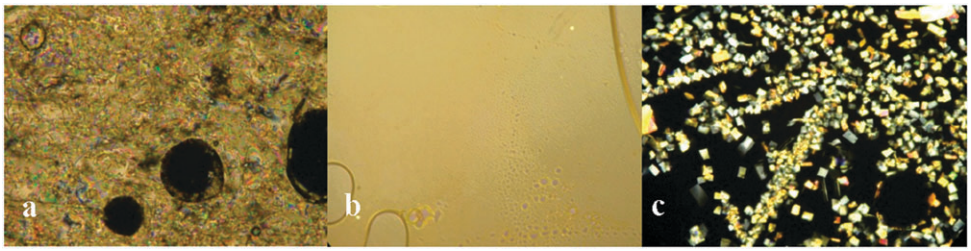

Fig. 4 Optical polarizing microscopic pictures (magnification 20×) of an MBBA–Ag NP conjugate prepared using 5 mol% $AgNO_3$: (a) before heating at room temperature, (b) isotropic mixture at 70 °C, and (c) on cooling to room temperature. The nematic texture of MBBA is lost and the final defect texture is retained in the film.

The phase separation is clearly visible before heating (a in Fig. 4). Upon heating, the mixture isotropizes (b in Fig. 4) and silver nanoparticles were generated. On cooling, no nematic texture was observed for mixtures containing 1–5 mol% $AgNO_3$. On the other hand, rectangular blocks were visible, which were aligned in a random fashion (c in Fig. 4). On re-heating, these rectangular blocks cleared to the isotropic phase and re-appeared on cooling. This unique defect texture was stable for several weeks. Interestingly, the LC property of the MBBA–Ag NP conjugate prepared using 80 mol% silver nitrate is entirely different from that of the other mixtures (Fig. 5). On heating to isotropic temperatures and cooling, bâtonnets structures were formed (Fig. 5c), which were then converted to focal conic smectic A texture (Fig. 5d). On rapid cooling, this mixture forms a stable glassy phase (Fig. 5e).

DSC studies were carried out to determine the phase transition temperatures in the above cases. Fig. 6 shows DSC thermograms obtained for MBBA and an MBBA–Ag NP conjugate prepared using 5 and 80 mol% $AgNO_3$. The MBBA–Ag NP conjugate showed higher transition temperatures compared to MBBA alone. Higher melting temperatures indicate the stabilization of the LC phase due to the presence of nanoparticles. The enthalpy change (ΔH) involving at the isotropization temperature also increases largely as the 'nematic' (less ordered) texture is changed to 'smectic' (highly ordered) [ΔH value for MBBA alone was 1.303 J g^{-1} and that for the MBBA–Ag NP conjugate (80 mol% $AgNO_3$) was 32.32 J g^{-1}].

Since conventional reducing agents are not utilized for reduction in the above systems, it is reasonable to assume that MBBA itself acts as the reducing agent. Nuclear magnetic resonance (NMR) experiments were performed for the MBBA–Ag NP conjugate in $CDCl_3$ to understand the structural changes in MBBA in association with the reduction of silver ions at different molar ratios. Fig. 7 shows the NMR spectra of an MBBA–Ag NP conjugate prepared using 5 and 80 mol% $AgNO_3$. The NMR spectra show the peaks correspond to 4-methoxybenzaldehyde and 4-butylaniline, which are the hydrolyzed products of MBBA, in addition to the peaks of un-dissociated MBBA. It was also noted that the percentage of both 4-methoxybenzaldehyde and 4-butylaniline was found to increase as the amount of the nanoparticle precursor ($AgNO_3$) was increased. For example, the integration values of the benzaldehyde (–CHO) peak (δ 9.9) and the MBBA imine (CH–N) peak (δ 8.4) exhibit a ratio of 1 : 5 for MBBA–Ag NP conjugate prepared using 5 mol% $AgNO_3$. The ratio was changed to 1 : 1 upon increasing the mole percentage of $AgNO_3$ to 80 mol% (Fig. 7b). Also, the ratio of the integration values for the alkyl protons of 4-butylaniline and MBBA increases in an identical manner. This clearly suggests that the dissociation of MBBA is closely associated with the reduction of $AgNO_3$.

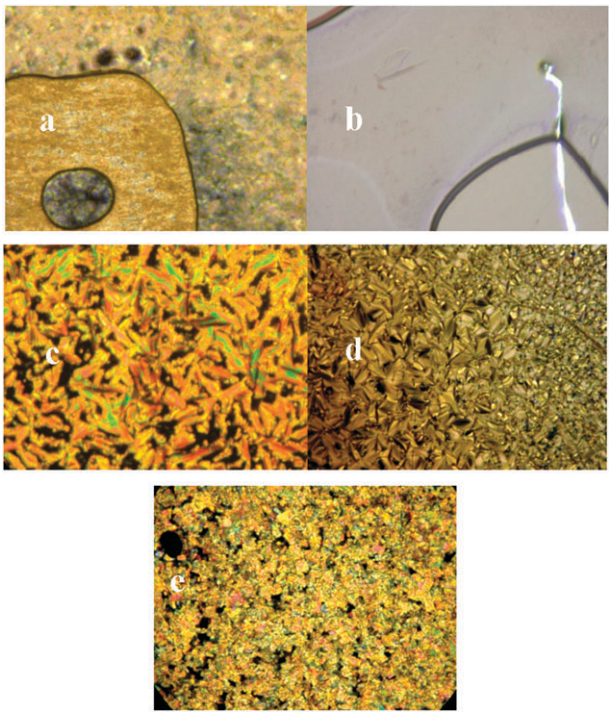

Fig. 5 Optical polarizing microscopic pictures (magnification 20×) of an MBBA–Ag NP conjugate prepared using 80 mol% $AgNO_3$: (a) before heating the mixture at room temperature, (b) isotropic phase of the mixture at 75 °C (c) Sm A bâtonnets structure at 73 °C in the cooling cycle, (d) focal conic Sm A texture at 70 °C in the cooling cycle and (e) glassy phase.

Imine-based reduction of silver ions has recently been reported in the literature.[20] It has also been reported that MBBA can be hydrolyzed to 4-methoxybenzaldehyde and 4-butylaniline in the presence of moisture, and the vertical alignment of 4-butylaniline results in lowering of the phase transition temperature of MBBA.[21] In the present case, complex formation of MBBA–Ag ions followed by reduction of silver ions by the imine moieties present in MBBA would be the initial steps, prior to the nucleophilic addition of water to

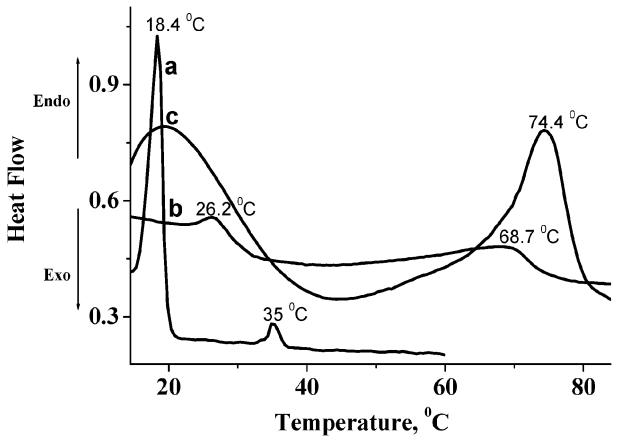

Fig. 6 DSC thermograms of (a) MBBA; MBBA–Ag NP conjugate prepared using (b) 5 mol%, and (c) 80 mol% $AgNO_3$ on heating cycle.

the imine bond which leads to the hydrolysis. The *in situ* formed silver nanoparticles catalyze the hydrolysis, which is evident from the fact that the extent of hydrolysis increases as the concentration of silver nanoparticle precursor increases. The mixture, which contains MBBA and its hydrolyzed products associated with the Ag nanoparticles, exhibit a layer ordered arrangement leading to the smectic texture. The important role of silver nanoparticles in the texture transformations is confirmed through control experiments, where equivalent amounts of MBBA, 4-methoxybenzaldehyde and 4-butylaniline were mixed and examined by OPM. The characteristic nematic texture of MBBA was found to be lost and no new texture formation was observed. The minimum amount of nanoparticle precursor required to transform the texture was found to be 40 mol% with respect to MBBA concentration. Further control experiments utilizing mixtures of 4-butylaniline and $AgNO_3$, as well as 4-methoxybenzaldehyde and $AgNO_3$, were examined through OPM, and no characteristic texture formation was observed. FT-IR studies showed a considerable shift in the stretching frequency of –C═N in MBBA (from 1625 to 1600 cm^{-1}), indicating significant coordination of MBBA molecules in the MBBA–Ag NP conjugate (please see Fig. S11 and S12 in the ESI†). The hydrolyzed products of MBBA were also strongly coordinated in the MBBA–Ag NP conjugate, as indicated by the FT-IR experimental results.

The MBBA–Ag NP conjugate can be obtained as a green powder at room temperature which is highly stable for several weeks. After two weeks, the green powder was examined under OPM and the images are given in Fig. 8.

The MBBA–Ag NP conjugate exhibits interesting emission properties upon photo-excitation at the silver plasmon absorption peak (420 nm) in the thin film. Fig. 9 contains the excitation and luminescence spectra of MBBA–Ag NP conjugate prepared using 80 mol% $AgNO_3$. The spectrum was taken after mixing and heat treating MBBA and $AgNO_3$ in required proportions. OPM analysis of these films was carried out and the formation of the glassy state was confirmed prior to the luminescence study. The emission maximum from the system with various molar ratios of silver ion precursor was at 500 nm.

In order to verify whether scattering from the metal nanoparticles has contributed to the luminescence signal in the present study, the excitation spectrum of the sample was taken and compared with that of the absorption spectrum. The remarkable similarity between the absorption and excitation maxima of the MBBA–Ag NP conjugate suggests that the contribution from scattering towards the signal intensity is negligible in the present case. The maximum intensity observed in the excitation spectrum was corresponding to the silver plasmon absorption, confirming that LC-embedded silver nanoparticles are responsible for the emission. Emission from silver nanoparticles stabilized in a polymer matrix has been reported previously and has been attributed to electronic transitions between the upper d band and the conducting sp band.[22] Emission from silver nanoparticles which are embedded in dendrimers and of size less than 3 nm was also reported in the literature.[23] A close examination of the HR-TEM images of the MBBA–Ag NP conjugate at higher molar ratios of $AgNO_3$ shows the uniform nanocasting of silver nanoparticles in the LC domain, which could be responsible for the emission in the system (Fig. 9, right). This is further substantiated by

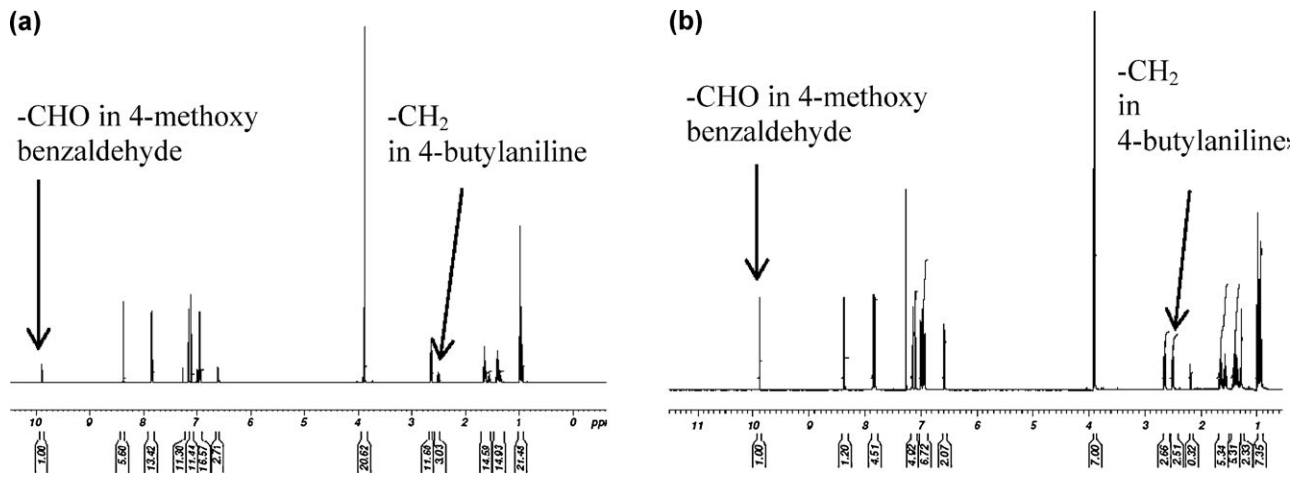

Fig. 7 ^1H NMR spectra of MBBA–Ag NP conjugate prepared using (a) 5 mol% $AgNO_3$ and (b) 80 mol% $AgNO_3$ after heat treatment. The signal intensity of the proton of 4-methoxybenzaldehyde increases as the $AgNO_3$ concentration increases.

Fig. 8 Optical polarizing microscopic pictures (magnification 20×) of an MBBA–Ag NP conjugate prepared using 80 mol% $AgNO_3$ (a) green powder obtained directly from the thin film, (b) isotropic phase of the mixture and (c) Sm A granular texture on cooling.

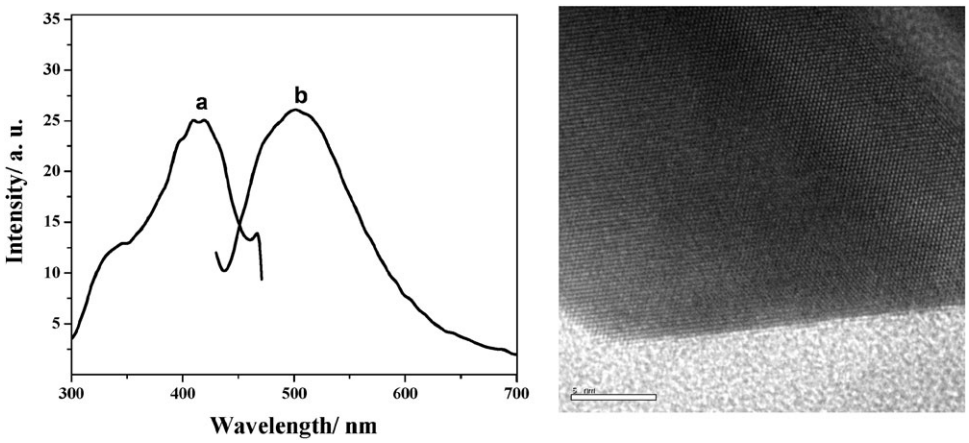

Fig. 9 Left: excitation (a) and emission (b) spectra of an MBBA–Ag NP conjugate in a thin film. For the emission spectrum, the excitation wavelength was 420 nm. For the excitation spectrum, emission was collected at 500 nm. 80 mol% $AgNO_3$ was used in this case. Right: HR-TEM image of MBBA–Ag NP conjugate powder showing the nanocasting (fcc packing) of silver. Scale: 5 nm.

the quenching of the luminescence intensity upon dissolution of the mixture in solvents, where the LC arrangement is not preserved.

Control experiments were also performed with (i) MBBA alone, (ii) a mixture of MBBA, 4-butylaniline and 4-methoxybenzaldehyde (1 : 1 molar ratio), and (iii) a mixture of 4-butylaniline and $AgNO_3$ in thin films (ESI, Fig. S9 and S10†). All of the control experiments resulted in the absence of luminescence at 500 nm upon excitation at 420 nm, indicating that the emission observed from the MBBA–Ag NP conjugate is unique and originated from the embedded silver nanoparticles in the LC domain. The luminescent, glassy, smectic MBBA–Ag NP conjugate was found to be highly stable, especially when prepared in polyvinyl alcohol-coated glass plates.

Conclusions

In the present study, we have investigated the silver nanoparticle-induced texture transformations in nematic MBBA through *in situ* formation of the metal nanoparticles in the LC domain. Based on the SEM, TEM, NMR and OPM results, we proposed that MBBA reduces silver ions to silver nanoparticles and the resulting MBBA–Ag NP conjugate exhibits a clear smectic texture. The formation of Ag nanoparticles in the mesogen leads to hydrolysis of a fraction of MBBA to 4-methoxybenzaldehyde and 4-butylaniline, followed by the ordered arrangement of MBBA and its hydrolyzed products on the nanoparticles. The material exhibits interesting luminescent properties in the LC state upon exciting the silver plasmon absorption peak. The results from the present study suggest that nano-scale molecular re-arrangements in liquid crystals can be utilized to generate distinct texture and optical properties for the host mesogen.

Experimental

Material

The nematic liquid crystal *N*-(4-methoxybenzylidene)-4-butylaniline (MBBA) was purchased from Aldrich. Dry methanol was prepared according to standard procedures.

Preparation of silver nanoparticles

Homogeneous solutions of MBBA (0.15 mmol) and silver nitrate (0.0015 mmol, 0.0045 mmol, 0.0075 mmol and 0.12 mmol) in 5 mL methanol were drop-cast onto a glass slide and the solvent was allowed to evaporate. The film thus formed was heated to isotropic temperature and kept at this temperature for 2 min. The sample was then cooled to room temperature. The NMR spectra of the MBBA–Ag NP conjugate were recorded on a Varian 500 MHz spectrometer using $CDCl_3$ as solvent.

Characterization of the LC

The phase transitions were observed under a polarizing optical microscope (Nikon Eclipse LV 100 POL) equipped with a locally made heating and cooling stage. DSC studies were carried out with a NETZSCH DSC 204 instrument operated

at a scanning rate of 10 °C min^{-1} under nitrogen atmosphere. For DSC studies, a homogeneous solution of the mesogen and silver nitrate in methanol, with different molar ratios, was drop-cast onto a glass plate, and the solvent was evaporated. The film thus formed was heated to isotropic temperatures to generate silver nanoparticles. The material was transferred to the DSC pan for measurements.

Characterization of silver nanoparticles

UV-Vis spectra of the silver nanoparticles formed in films were recorded on a Perkin-Elmer Lambda 25 UV-Visible Spectrophotometer. The films containing silver nanoparticles in LC matrix were directly inserted into the UV-Vis spectrophotometer and the spectrum was recorded while keeping a plain glass plate as reference. The powder X-ray diffraction study was carried out for MBBA–Ag NP conjugate (80 mol% $AgNO_3$) powder on a Bruker AXS-D8 diffractometer (Cu cathode) equipped with a Lynx detector. Transmission electron microscopy (TEM) images were recorded by using JEM 3010 JEOL, operated at 200 kV. A homogeneous solution of mesogen and silver nitrate in methanol was drop-cast onto a Cu grid. The solvent was allowed to evaporate. After drying the grid, the sample was heated on a heating stage to obtain isotropic temperature. The grid was allowed to cool and examined under an electron microscope. SEM studies were carried out using an FEI: QUANTA scanning electron microscope, utilizing a silicon wafer for casting the sample.

Fluorescence study

The luminescence properties (excitation and emission spectra) of the MBBA–Ag NP conjugate were studied in a Fluoromax®-4 (Horiba Jobin Yvon, USA) spectrofluorimeter. The MBBA–Ag NP conjugate film with various molar ratios of $AgNO_3$ was inserted into the fluorimeter and the emission was collected at an angle of 60 °C, using the solid-state luminescence measurement set up in Fluoromax®-4.

Acknowledgements

P. K. S. Antharjanam thanks the Department of Science and Technology (DST) for the financial support through FAST TRACK scheme (No.SR/FTP/CS-127/2006). The authors thank Professor T. Pradeep, IIT Madras for HR-TEM images, Dr K. V. Rama, SAIF, IIT Madras for DSC analysis, and the Department of Metallurgical and Materials Engineering, IIT Madras for HR-SEM images and XRD analysis.

References

1 K. Robbie, D. J. Broer and M. J. Brett, *Nature*, 1999, **399**, 764.
2 H. Qi and T. Hegmann, *J. Mater. Chem.*, 2006, **16**, 4197; T. Hegmann, H. Qi and V. M. Marx, *J. Inorg. Organomet. Polym. Mater.*, 2007, **17**, 483, and references therein.
3 L. Cseh and G. H. Mehl, *J. Am. Chem. Soc.*, 2006, **128**, 13376.
4 M. Mitov, C. Portet, C. Bourgerette, E. Snoeck and M. Verelst, *Nat. Mater.*, 2002, **1**, 229.
5 B. V. Barmatov, D. A. Pebalk and M. V. Bamatova, *Langmuir*, 2004, **20**, 10868.
6 C. Da Cruz, O. Sandre and V. Cabuil, *J. Phys. Chem. B*, 2005, **109**, 14292.
7 M. Yamada, Z. Shen and M. Miyake, *Chem. Commun.*, 2006, 2569.
8 C. Da Cruz, O. Sandre and V. Cabuil, *J. Phys. Chem. B*, 2005, **109**, 14292.
9 Y.-H. Chen and W. Lee, *Appl. Phys. Lett.*, 2006, **88**, 222105.
10 V. A. Mallia, P. K. Vemula, G. John, A. Kumar and P. M. Ajayan, *Angew. Chem., Int. Ed.*, 2007, **46**, 3269.
11 D. T. McCormick, R. Chavers and C. A. Guymon, *Macromolecules*, 2001, **34**, 6929.
12 W. Dobbs, J.-M. Suisse, L. Douce and R. Welter, *Angew. Chem., Int. Ed.*, 2006, **45**, 4179.
13 N. E. Domracheva, A. Mirea, M. Schwoerer, L. L. Torre and G. Lattermann, *ChemPhysChem*, 2006, **7**, 2567.
14 H. Qi and T. Hegmann, *J. Mater. Chem.*, 2008, **18**, 3288.
15 L. Huang, H. Wang, Z. Wang, A. Mitra, K. N. Bozhilov and Y. Yan, *Adv. Mater.*, 2002, **14**, 61; R. Patakfalvi and I. Dékány, *Colloid Polym. Sci.*, 2002, **280**, 461; F. Bouchama, M. B. Thathagar, G. Rothenberg, D. H. Turkenburg and E. Eiser, *Langmuir*, 2004, **20**, 477; M. Andersson, V. Alfredsson, P. Kjellin and A. E. C. Palmqvist, *Nano Lett.*, 2002, **2**, 1403.
16 (*a*) E. B. Barmatov, D. A. Pebalk and M. V. Barmatova, *Langmuir*, 2004, **20**, 10868; (*b*) N. A. Nikonorova, E. B. Barmatocv, D. A. Pebalk, M. B. Barmatova, G. Dominguez-Espinosa, R. Diaz-Calleja and P. Pissis, *J. Phys. Chem. C*, 2007, **111**, 8451; (*c*) N. Nishida, Y. Shiraishi, S. Kobayashi and N. Toshima, *J. Phys. Chem. C*, 2008, **112**, 20284.
17 J. D. S. Newman and G. J. Blanchard, *Langmuir*, 2006, **22**, 5882; M. Chen, Y.-G. Feng, X. Wang, T.-C. Li, J.-Y. Zhang and D.-J. Qian, *Langmuir*, 2007, **23**, 5296.
18 S. Kéki, J. Török, G. Deák, L. Daróczi and M. Zsuga, *J. Colloid Interface Sci.*, 2000, **229**, 550.
19 L. Huang, H. Wang, Z. Wang, A. Mitra, K. N. Bozhilov and Y. Yan, *Adv. Mater.*, 2002, **14**, 61.
20 The *in situ* reduction of silver ions by mesoporous materials containing grafted imines has recently been reported: Y. Xie, S. Quinlivan and T. Asefa, *J. Phys. Chem. C*, 2008, **112**, 9996.
21 *Liquid Crystals: Applications and Uses*, ed. B. Bahadur, World Scientific Pub. Co. Inc., New Jersey, USA, 1990.
22 J. Gao, J. Fu, C. Lin, Y. Han, X. Yu and C. Pan, *Langmuir*, 2004, **20**, 9775, and references therein.
23 J. Zheng and R. M. Dikson, *J. Am. Chem. Soc.*, 2002, **124**, 13982.